

SEARCH FOR [CII] EMISSION IN $Z = 6.5 - 11$ STAR-FORMING GALAXIES.

JORGE GONZÁLEZ-LÓPEZ^{1,3,9}, DOMINIK A. RIECHERS², ROBERTO DECARLI³, FABIAN WALTER³, LIVIA VALLINI⁴, ROBERTO NERI⁵, FRANK BERTOLDI⁶, ALBERTO D. BOLATTO⁷, CHRISTOPHER L. CARILLI⁸, PIERRE COX⁵, ELISABETE DA CUNHA³, ANDREA FERRARA⁴, SIMONA GALLERANI⁴, AND LEOPOLDO INFANTE^{1,9}

Accepted for publication in the Astrophysical Journal.

ABSTRACT

We present the search for the [C II] emission line in three $z > 6.5$ Lyman-alpha emitters (LAEs) and one J-Dropout galaxy using the Combined Array for Research in Millimeter-wave Astronomy (CARMA) and the Plateau de Bure Interferometer (PdBI). We observed three bright $z \sim 6.5 - 7$ LAEs discovered in the SUBARU deep field (SDF) and the Multiple Imaged lensed $z \sim 11$ galaxy candidate found behind the galaxy cluster MACSJ0647.7+7015. For the LAEs IOK-1 ($z = 6.965$), SDF J132415.7+273058 ($z = 6.541$) and SDF J132408.3+271543 ($z = 6.554$) we find upper limits for the [C II] line luminosity of < 2.05 , < 4.52 and $< 10.56 \times 10^8 L_{\odot}$ respectively. We find upper limits to the FIR luminosity of the galaxies using a spectral energy distribution template of the local galaxy NGC 6946 and taking into account the effects of the Cosmic Microwave Background on the mm observations. For IOK-1, SDF J132415.7+273058 and SDF J132408.3+271543 we find upper limits for the FIR luminosity of < 2.33 , 3.79 and $7.72 \times 10^{11} L_{\odot}$ respectively. For the lensed galaxy MACS0647-JD, one of the highest redshift galaxy candidate to date with $z_{\text{ph}} = 10.7^{+0.6}_{-0.4}$ we put an upper limit in the [C II] emission of $< 1.36 \times 10^8 \times (\mu/15)^{-1} L_{\odot}$ and an upper limit in the FIR luminosity of $< 6.1 \times 10^{10} \times (\mu/15)^{-1} L_{\odot}$ (where μ is the magnification factor). We explore the different conditions relevant for the search for [C II] emission in high redshift galaxies as well as the difficulties for future observations with ALMA and CCAT.

Keywords: galaxies: high-redshift– galaxies: individual (IOK-1, SDF J132415.7+273058, SDF J132408.3+271543, MACS0647-JD) –ISM: lines and bands

1. INTRODUCTION

Lyman-alpha Emitters (LAE) are galaxies selected through strong Ly α emission and are among the most studied galaxy populations at high redshift. The use of narrow band filters over a wide area on the sky has proven to be a very effective method to find galaxies up to $z \sim 7$ (Iye et al. 2006; Fontana et al. 2010; Vanzella et al. 2011; Rhoads et al. 2012; Shibuya et al. 2012; Schenker et al. 2012; Ono et al. 2012). The possibility of finding LAEs from $z \sim 1$ to $z \sim 7$ shows that this type of galaxies can be used to understand galaxy evolution over cosmic time. It has been observed that the LAE fraction in UV selected galaxies increases with redshift up to $z \sim 6$ (Stark et al. 2010), which is expected due to the decreasing dust content at higher redshifts. Beyond $z \sim 6$ it is

expected that the LAE fraction decreases as the amount of neutral Hydrogen (H I) increases, due to the incomplete reionization of the Intergalactic Medium (IGM) (Ota et al. 2008; Stark et al. 2010; Pentericci et al. 2011; Ono et al. 2012; Schenker et al. 2012). This is consistent with the comparatively low success rate of detection of Ly α emission at $z \gtrsim 7$.

If Lyman-alpha photons from redshifts $z \geq 7$ are absorbed by H I in the IGM (Dayal & Ferrara 2012), it will be difficult to spectroscopically confirm the candidates at high redshift, such as the candidate $z \sim 12$ galaxy UDFj-39546284 discovered in the Hubble Space Telescope (HST) Ultra Deep Field (UDF) (Bouwens et al. 2011; Ellis et al. 2013; Brammer et al. 2013; Capak et al. 2013), and the candidates found behind galaxy clusters at $z \sim 9.6$ MACS1149-JD and ~ 10.7 MACS0647-JD (Zheng et al. 2012; Coe et al. 2013).

Among the usual Interstellar medium (ISM) tracers at optical/UV wavelengths, the only line that has been observed at $z > 4$ in galaxies is Ly-alpha. The emission of Ly-alpha is complicated by its high optical depth in the emission region and its escape through resonant scattering, by dust absorption, and by the contribution from outflows. Therefore direct constraints on the gas properties from the Ly-alpha line strength and shape are difficult to derive. This motivates the exploration of alternative means to study the highest redshift galaxies. Promising candidates include far-infrared fine structure emission lines, e.g., [C II] ($^2P_{3/2} \rightarrow ^2P_{1/2}$) at $157.74 \mu\text{m}$, which is not affected by the increasingly neutral IGM at $z > 7$ and can account for up to 1% of the total infrared luminosity in some galax-

¹ Instituto de Astrofísica, Facultad de Física, Pontificia Universidad Católica de Chile, Av. Vicuña Mackenna 4860, 782-0436 Macul, Santiago, Chile; jgonzal@astro.puc.cl

² Astronomy Department, Cornell University, 220 Space Sciences Building, Ithaca, NY 14853, USA

³ Max Planck Institute für Astronomie Heidelberg, Königstuhl 17, D-69117 Heidelberg, Germany

⁴ Scuola Normale Superiore, Piazza dei Cavalieri 7, I-56126 Pisa, Italy

⁵ Institut de RadioAstronomie Millimétrique, 300 Rue de la Piscine, Domaine Universitaire, 38406 Saint Martin d'Hères, France

⁶ Argelander Institute for Astronomy, University of Bonn, Auf dem Hügel 71, 53121 Bonn, Germany

⁷ Department of Astronomy, University of Maryland, College Park, MD 20742, USA

⁸ National Radio Astronomy Observatory, P. O. Box 0, Socorro, NM 87801, USA

⁹ Centro de Astro-Ingeniería, Pontificia Universidad Católica de Chile, V. Mackenna 4860, Santiago, Chile

ies, especially in those with low luminosity and metallicity (Crawford et al. 1985; Stacey et al. 1991; Israel et al. 1996; Madden et al. 1997).

The [C II] line traces photo-dissociation (a.k.a. photon-dominated) regions (PDRs), as well as diffuse H I and H II regions. In PDRs, the far-UV radiation produced by OB stars heats the surface layers of molecular clouds, which cool preferentially through [C II] emission. It has been observed that most of the [C II] emission in IR-bright galaxies is coming from PDRs, and that the PDR gas mass fraction can be up to 50% in starbursts like M82 (Crawford et al. 1985).

Modeling of FIR emission lines observed in starburst galaxies showed that at least 70% of the [C II] emission is produced in PDRs (Carral et al. 1994; Lord et al. 1996; Colbert et al. 1999). In the low-metallicity system Haro 11, on the other hand, at least 50% of the [C II] emission arises from a more diffuse, extended ionized medium (Cormier et al. 2012). The different conditions in which the [C II] emission is produced, and the direct or indirect relation of these conditions with the star formation process, suggest that [C II] emission should be a good tracer of the global galactic star formation activity (de Looze et al. 2011), at least for galaxies with low T_{dust} or low $\Sigma_{\text{IR}} = L_{\text{IR}}/\pi r_{\text{mid-IR}}^2$ (Diaz-Santos et al. 2013). [C II] is found to be the strongest emission line, stronger than CO, and thus is the most promising tracer of the dense, star forming regions in distant galaxies where [C II] can be detected with ground-based telescopes due to the redshift into observable atmospheric windows.

In the past years, the [C II] 158 μm emission line has been established as a promising observable in high-redshift galaxies (Maiolino et al. 2005; Iono et al. 2006; Maiolino et al. 2009; Walter et al. 2009; Hailey-Dunsheath et al. 2010; Stacey et al. 2010; Ivison et al. 2010; Wagg et al. 2010; Cox et al. 2011; De Breuck et al. 2011; Valtchanov et al. 2011; Gallerani et al. 2012; Venemans et al. 2012; Wagg et al. 2012; Walter et al. 2012a; Carilli et al. 2013; Wang et al. 2013; Willott et al. 2013; Riechers et al. 2013). Most of the high- z detections were for infrared-luminous starbursts, many of which also show signatures of AGN. See the review by Carilli & Walter (2013) for more details.

With star formation rates of a few tens $\text{M}_{\odot}\text{yr}^{-1}$, based on the Ly α and UV continuum emission, LAEs are classified as “normal” star forming galaxies. Different studies claim that LAEs are young, dust free, starbursting galaxies, supported by UV observations (Gawiser et al. 2006; Finkelstein et al. 2007; Lai et al. 2008). Recent MIR detection of LAEs at $z \sim 2.5$ and $z < 0.3$ show that a significant fraction of the star formation in these galaxies is strongly obscured by dust (Oteo et al. 2012a,b). Thus, LAEs are promising targets for the detection of [C II] at high redshift.

Previous attempts to detect [C II] in a small sample of LAEs at $z \sim 6.6$ were unsuccessful (Walter et al. 2012b; Kanekar et al. 2013; Ouchi et al. 2013).

Here we present the result of a search for [C II] in three LAEs at $z > 6.5$ and in a lensed galaxy at $z \sim 11$. In Sect. 2 we describe the target selection and observations. The data is shown in Sect. 3 together with some implications and analysis in Sect. 4. A summary of the paper

is presented in Sect. 5. Throughout this paper we use a Λ -Cold Dark Matter cosmology with $H_0 = 70 \text{ km s}^{-1} \text{ Mpc}^{-1}$, $\Omega_{\Lambda} = 0.7$ and $\Omega_{\text{m}} = 0.3$.

2. OBSERVATIONS

2.1. Source Selection

The three Lyman- α emitters targeted in this study were discovered in the Subaru Deep Field (SDF). Two of the LAEs observed belong to the sample of LAEs at $z \sim 6.6$ discovered by Taniguchi et al. (2005). The targets are the brightest LAEs (sources 3 and 4 in their catalog) and have a narrow and bright Lyman- α emission line. The third LAE (IOK-1) was discovered at $z \sim 7$ by Iye et al. (2006). It is one of the brightest and most distant LAEs known to date.

The fourth target, MACS0647-JD, is a lensed Lyman-break galaxy (LBG) discovered behind the galaxy cluster MACSJ0647.7+7015 at $z = 0.591$ (Coe et al. 2013). The galaxy was discovered as a J-Dropout galaxy lensed into 3 magnified images as part of The Cluster Lensing And Supernova survey with Hubble (CLASH) (Postman et al. 2012). The three images of the galaxy MACS0647-JD1, MACS0647-JD2 and MACS0647-JD3, have a magnification of ~ 8 , ~ 7 and ~ 2 respectively. The photometric redshift of the galaxy is $10.7^{+0.6}_{-0.4}$ (95% confidence limits). This is one of the highest redshift galaxy candidates known to date.

2.2. CARMA Observations

Observations of the three $z \sim 6.5 - 7$ LAEs were carried out using the Combined Array for Research in Millimeter-wave Astronomy (CARMA) between 2008 July and 2010 July. The array configurations used were the most compact, D and E, to minimize phase decoherence and maximize point source sensitivity. The [C II] line has a rest frequency of 1900.54 GHz (157.74 μm). For the redshifts of the targets, the line is shifted to the 1 mm band. The receivers were tuned to a frequency $\sim 150 \text{ km s}^{-1}$ bluer than the expected frequency from the redshift determined by the peak of the Lyman- α line. This is for taking into account the possible absorption by the IGM in the Lyman- α line. The setups provide an instantaneous bandwidth of $\sim 1.5 \text{ GHz}$ ($\sim 1800 \text{ km s}^{-1}$) with a spectral resolution of 31.25 MHz ($\sim 37 - 39 \text{ km s}^{-1}$).

The observations were processed using MIRIAD (Sault et al. 1995). The absolute flux calibrators used are 3C84, MWC349, 3C273 and Mars, the latter being the most used. As passband calibrators the QSOs 3C273, 3C345 and 0854+201 were used. As gain calibrator the QSO 1310+323 was used. The time on source for IOK-1 was 58.5 hours, for SDF J132415.7+273058 was 15.9 hours and for SDF J132408.3+271543 4.6 hours. The final cubes were made using natural weighting to maximize point source sensitivity. The observations resulted in the following beamsizes: IOK-1: $1.86'' \times 1.33''$, PA = -0.34° , SDF J132415.7+273058: $1.92'' \times 1.56''$, PA = 83.45° , SDF J132408.3+271543: $2.54'' \times 2.01''$, PA = 88.02° (all targets: D and E configurations). For D configuration the minimum baseline is 11 meters and the maximum is 150 meters. For E configuration the minimum baseline is 8 meters and the maximum is 66 meters. Table 1 summarizes the sensitivities reached for the observations of the LAEs.

2.3. PdBI Observations

All MACS0647-JD observations were carried out in 2012 November as part of a DDT (Director's Discretionary Time) program with the Plateau de Bure Interferometer (PdBI). The target was observed with 4 WideX frequency setups (3.6 GHz bandwidth each), covering 80% of the photometric redshift range ($z = 10.1 - 11.1$). Two of the three lensed images (JD1 and JD2) are within $18''$ of each other and they were covered in a common 2 mm pointing. The absolute flux calibrators used are MWC349, 2200+420, 3C279 and 0716+714. As gain calibrator the QSO 0716+714 was used. The total on source time for all tunings was 7.4 hours (6-antennas equivalent). The observations were processed using GILDAS. The beamsize of the observations is the following: MACS0647-JD : $2.10'' \times 1.76''$, PA= 102.0° (C configuration). For C configuration the minimum baseline is 22 meters and the maximum is 184 meters. Table 2 summarizes the sensitivity reached for the observations of MACS0647-JD .

3. RESULTS

3.1. Line Emission

The spectra of the three $z \sim 6.5 - 7$ LAEs are presented in Fig. 1 and the spectrum of MACS0647-JD is shown in Fig. 2. No significant emission is detected at the redshifted line frequencies or close to them. The observations were sampled to a channel resolution of 50 km s^{-1} similar to the expected FWHM of the [CII] emission line (see Sect. 4.1). We use our non-detections to put constraints on the luminosities of the [CII] lines for all targets. The results for the LAEs can be seen in the Table 1 and for the MACS0647-JD in Table 2. The upper limits were estimated assuming that the sources were unresolved. For MACS0647-JD the spectra of the two images were corrected by the primary beam pattern before combination. The [CII] luminosities were estimated assuming that the velocity integrated flux of the line is $I_{\text{line}} = S_{\text{line}} \Delta v$, with S_{line} being 3 times the r.m.s. of the 50 km s^{-1} channel and $\Delta v = 50 \text{ km s}^{-1}$ the range in velocity (details on Tab. 1 notes). Using 3σ over a 50 km s^{-1} channel to estimate the upper limit in the luminosities can result in an underestimation. We point out that for a more conservative estimation the luminosities should be multiplied by a factor 2. (i.e. 3σ over 200 km s^{-1} channel). Assuming a channel width of 200 km s^{-1} , our IOK-1 [CII] limit is $\sim 10\%$ deeper than the previous PdBI limit (Walter et al. 2012b).

3.2. Continuum Emission

No continuum emission is detected in our observations of the three LAEs and the $z \sim 11$ LBG. The sensitivity reached for the continuum observations is given in the Tab. 1 for the LAEs and a continuum map for the three LAEs is shown in Fig. 3. The results for the MACS0647-JD are given in Tab. 2 and the continuum map is shown in Fig. 4. In Sect. 4.2 we discuss how the CMB affects our continuum observations and in Sect. 4.3 we use our continuum measurements to constrain the nature of our targets.

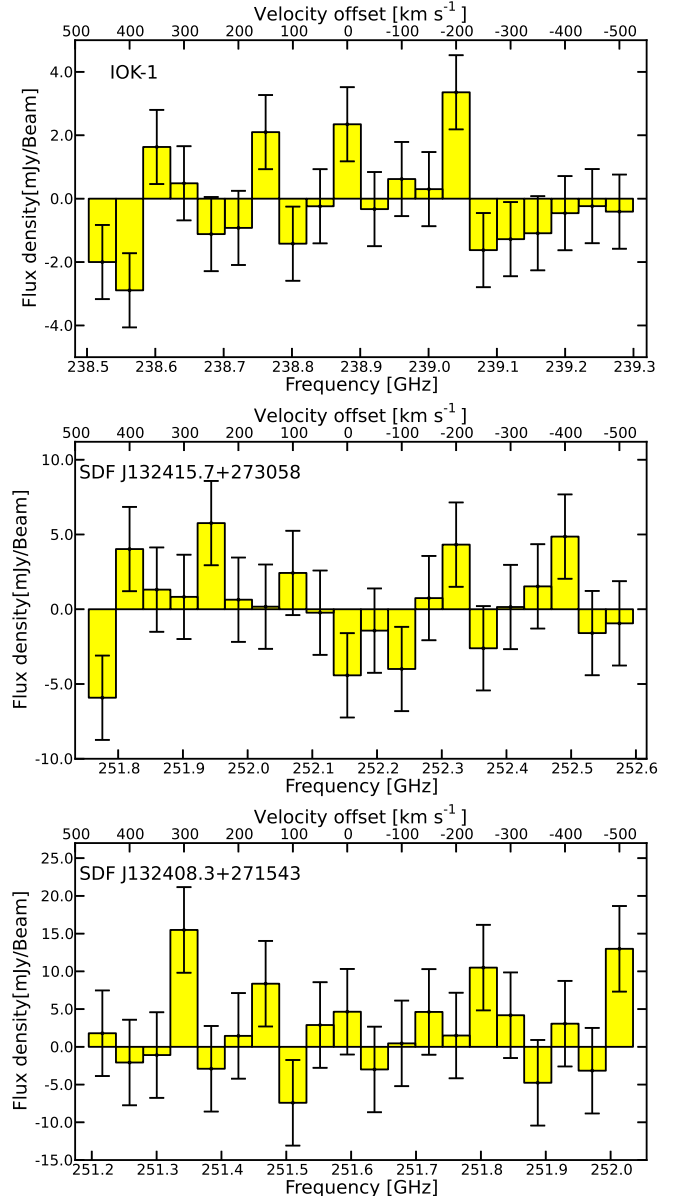


Figure 1. Spectra of the LAEs with a velocity resolution of 50 km s^{-1} . The relative velocities are with respect to the frequency expected for the [CII] line including absorption by the IGM (150 km s^{-1} to the blue of $z_{\text{Ly}\alpha}$). The redshifts of the target are $z=6.965$ for IOK-1, $z=6.541$ for SDF J132415.7+273058 and $z=6.554$ for SDF J132408.3+271543 .

4. DISCUSSION

4.1. Width of the [CII] emission line.

Previous studies have presented the non-detection of [CII] (Walter et al. 2012b; Ouchi et al. 2013) with a channel resolution of 200 km s^{-1} , a choice motivated by the width of the Ly α emission line. We argue that recent observations and models of [CII] in LAEs suggest that the [CII] line could be narrower than the previously assumed value.

4.1.1. [CII] detection on a LAE $z=4.7$.

In support of a narrow emission line is the detection of [CII] in a LAE at $z = 4.7$ (Ly α -1) with ALMA (Carilli et al. 2013). The FWHM of the emis-

Table 1
Summary of Observations and Results for the LAEs

source	RA J2000.0	DEC J2000.0	z^a	ν_{obs}^b GHz	σ_{cont}^c mJy b^{-1}	σ_{line}^d mJy b^{-1}	$L_{[\text{CII}]}^e$ $10^8 L_{\odot}$	$L_{\text{IR,CMB}}^{N6946,f}$ $10^{11} L_{\odot}$	$\text{SFR}_{\text{dust,CMB}}^g$ $M_{\odot} \text{ yr}^{-1}$	SFR_{UV}^h $M_{\odot} \text{ yr}^{-1}$
IOK-1	13:23:59.80	+27:24:56.0	6.965	238.881	0.19	1.17	<2.05	<6.34	<109.1	~24
SDF J132415.7	13:24:15.70	+27:30:58.0	6.541	252.154	0.37	2.82	<4.52	<10.3	<177.2	~34
SDF J132408.3	13:24:08.30	+27:15:43.0	6.554	251.594	0.75	5.67	<10.56	<21.0	<360.9	~15

Note. — All luminosities upper limits are 3σ .

^a References: IOK-1: Iye et al. (2006); Ono et al. (2012) –SDF J132415.7+273058 and SDF J132408.3+271543 : Taniguchi et al. (2005)

^b Observing Frequencies; tuned ~ 125 MHz blueward of the Ly- α redshifts for all targets.

^c 1σ continuum sensitivity at $158\mu\text{m}$ rest wavelength.

^d 1σ [CII] line sensitivity over a channel width of 50 km s^{-1} .

^e 3σ [CII] luminosity limit over a channel width of 50 km s^{-1} assuming $L_{\text{line}} = 1.04 \times 10^{-3} I_{\text{line}} \nu_{\text{rest}} (1+z)^{-1} D_L^2$, where the line luminosity, L_{line} , is measured in L_{\odot} ; the velocity integrated flux, $I_{\text{line}} = S_{\text{line}} \Delta v$, in Jy km s^{-1} ; the rest frequency, $\nu_{\text{rest}} = \nu_{\text{obs}} (1+z)$, in GHz; and the luminosity distance, D_L , in Mpc. (e.g. Solomon et al. (1992))

^f 3σ limit based on the SED of NGC 6946 and including the effect of the CMB.

^g 3σ limit based on L_{IR}^{N6946} including the effect of the CMB.

^h UV-based SFR from Jiang et al. (2013a)

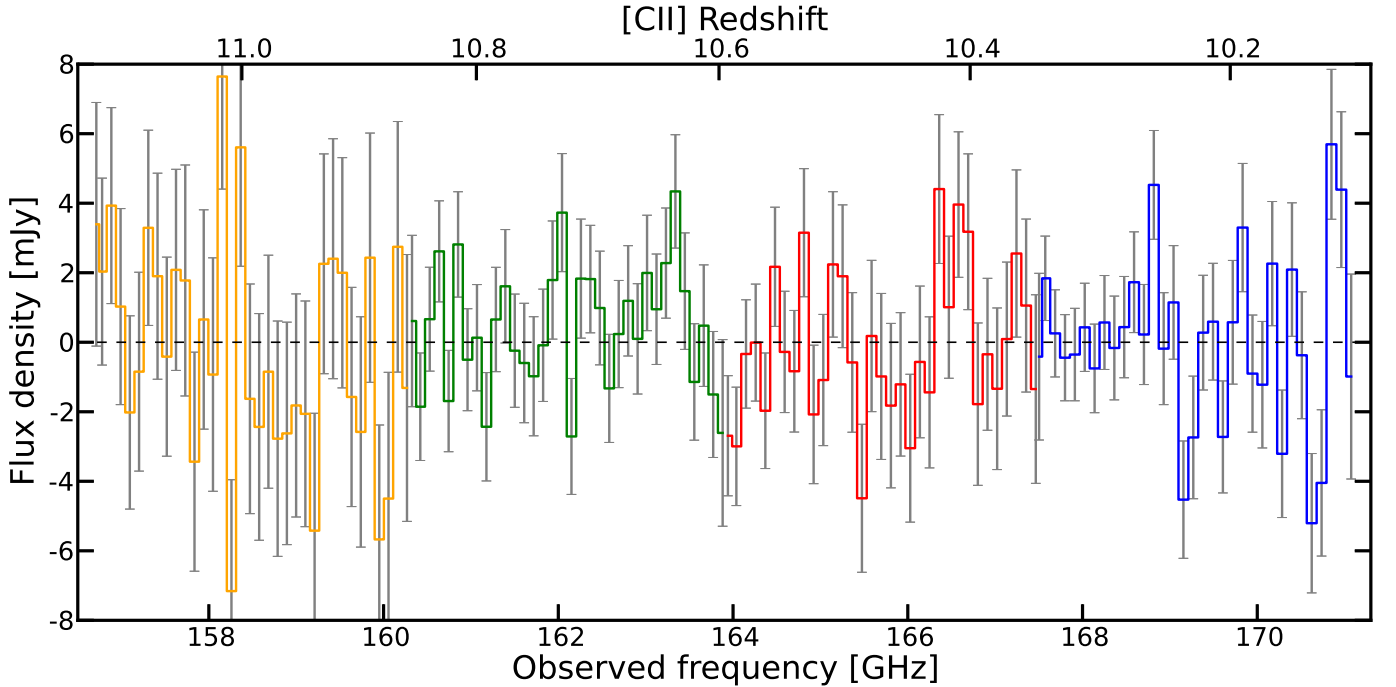


Figure 2. Spectrum of MACS0647-JD. The spectrum shows the added fluxes measured on the positions of the two lensed images JD1 and JD2 (combined magnification $\mu \sim 15$). The spectra of the two images were corrected by the primary beam pattern before combination. The 4 setups are plotted in different colors, blue, red, green and orange the colors for the setups A, B, C and D respectively. The error bars correspond to the quadrature of the errors of the individual measurement of the fluxes for JD1 and JD2 in each frequency channel. For display purposes, the spectrum is sampled at a channel resolution of 200 km s^{-1} , but the search of the [CII] line as well as the analysis was made with the spectrum sampled to 50 km s^{-1} .

sion line is 56 km s^{-1} , which is one order of magnitude narrower than the width of the Ly α emission line of $\sim 1100 \text{ km s}^{-1}$ of the same source (Petitjean et al. 1996; Ohyama et al. 2004). Despite of the LAE being at a separation of $2.3''$ ($\sim 15 \text{ kpc}$) to the quasar BRI 1202-0725, there is no evidence for a significant influence of the quasar on the properties of the LAE from the observations. Carilli et al. (2013) tried to model the emission of the LAE taking into account the radiation coming from the luminous nearby quasar. All the models that reproduce the [CII] and Ly α luminosities predict higher luminosities for other UV lines that are not detected (Ohyama et al. 2004). Given this results, they

conclude that the quasar is unlikely the source of heating and ionization in the LAE.

Based on deep, spatially resolved optical spectroscopy of the LAE, Ohyama et al. (2004) argue that the LAE is likely the composition of a normal star-forming galaxy and an extended nebula with violent kinematic status. This nebula emission would produce a broadening of the Ly α emission. This nebula can be explained, at least in a qualitative way, as a superwind caused by the supernovae explosion of OB stars in the late phase of the evolution of a starburst.

In conclusion, this LAE is not intrinsically different from the general population of LAE. The [CII] detection

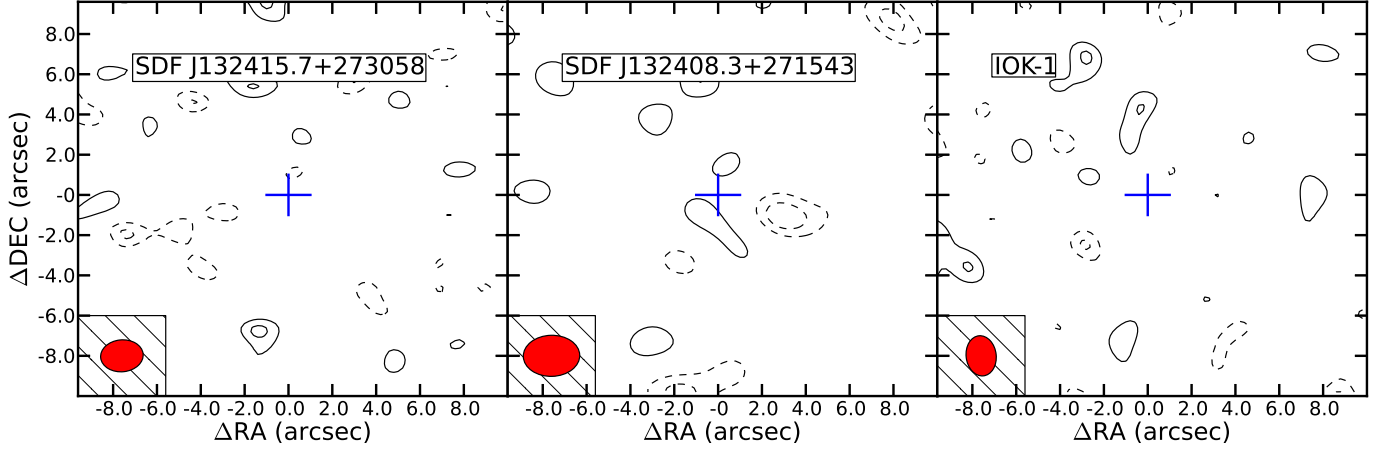


Figure 3. Rest-frame $158 \mu\text{m}$ continuum maps of the LAEs. Each contour level represents 1σ steps ($\pm 1\sigma$ levels are not shown). Solid contours are positive signal and dashed contour are negative signals. The 1σ levels are $0.75 \text{ mJy beam}^{-1}$ for SDF J132408.3+271543, $0.37 \text{ mJy beam}^{-1}$ for SDF J132415.7+273058 and $0.19 \text{ mJy beam}^{-1}$ for IOK-1. The blue crosses represent the position of each LAE as given in Tab. 1.

Table 2
Summary of Observations and Results for MACS0647JD

Parameter	MACS0647-JD1, JD2
Coordinates (J2000) JD1	06:47:55.731,+70:14:35.76
Coordinates (J2000) JD2	06:47:53.112,+70:14:22.94
μ (JD1+JD2)	~ 15
Redshift	$10.7^{+0.6}_{-0.4}$
UV SFR	$\sim 1 [\text{M}_{\odot} \text{yr}^{-1}]$
ν	$156.7\text{--}171.1 [\text{GHz}]$
σ_{cont}^a	$0.17 \text{ mJy beam}^{-1}$
σ_{line} (Setup A) ^b	$3.31 \text{ mJy beam}^{-1}$
σ_{line} (Setup B) ^b	$4.12 \text{ mJy beam}^{-1}$
σ_{line} (Setup C) ^b	$3.19 \text{ mJy beam}^{-1}$
σ_{line} (Setup D) ^b	$6.42 \text{ mJy beam}^{-1}$
$L_{[\text{CII}]}$ (Setup C) ^c	$< 6.78 \times 10^7 \times (\mu/15)^{-1} [\text{L}_{\odot}]$
$L_{[\text{CII}]}$ (Setup D) ^c	$< 1.36 \times 10^8 \times (\mu/15)^{-1} [\text{L}_{\odot}]$
$L_{\text{IR}}^{\text{N6946,d}}$ (Corrected CMB)	$< 1.65 \times 10^{11} \times (\mu/15)^{-1} [\text{L}_{\odot}]$
SFR (L_{IR}) (Corrected CMB) ^e	$< 28 \times (\mu/15)^{-1} [\text{M}_{\odot} \text{yr}^{-1}]$
SFR ($L_{[\text{CII}]}$) (Setup C) ^f	$< 5 \times (\mu/15)^{-1} [\text{M}_{\odot} \text{yr}^{-1}]$
SFR ($L_{[\text{CII}]}$) (Setup D) ^f	$< 9 \times (\mu/15)^{-1} [\text{M}_{\odot} \text{yr}^{-1}]$

Note. — All luminosities upper limits are 3σ .

References: Coordinates, magnification, redshift and UV-SFR from Coe et al. 2013.

All the luminosities and SFR are corrected by magnification.

^a 1σ continuum sensitivity at $158\mu\text{m}$ rest wavelength.

^b 1σ [CII] line sensitivity over a channel width of 50 km s^{-1} .

^c 3σ [CII] luminosity limit over a channel width of 50 km s^{-1} as in Tab. 1. The two results correspond to the most sensitive and the least sensitive setups.

^d 3σ limit based on the SED of NGC 6946 and including the effect of the CMB.

^e 3σ limit based on $L_{\text{IR}}^{\text{N6946}}$ including the effect of the CMB.

^f Based on the De Looze et al., 2011 $L_{[\text{CII}]} - \text{SFR}$ relation. The two results correspond to the most sensitive and the least sensitive setups.

in this LAE can thus be used as a reference for [CII] searches in other LAEs at high redshift.

4.1.2. Himiko simulations.

Simulations also suggest narrow [CII] emission lines at high redshift for LAEs. Vallini et al. (2013) combine a high resolution cosmological simulation with a sub-grid multi-phase model of the interstellar medium to simulate the [CII] emission in a halo similar to the LAE Himiko at $z = 6.6$. They find that 95% of the [CII] emission is generated in the Cold Neutral Medium (CNM), mainly in

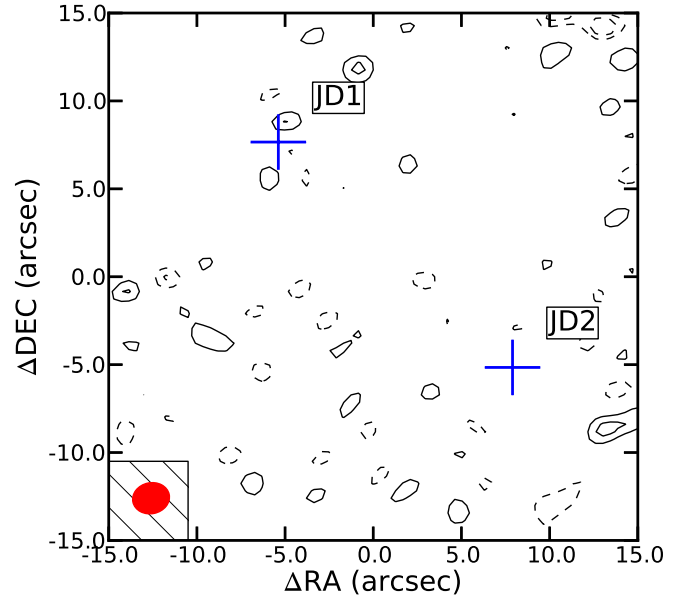


Figure 4. Continuum map of the field of MACS0647-JD. Each contour level represents 1σ steps ($\pm 1\sigma$ levels are not shown). Solid contours are positive signal and dashed contour are negative signals. The 1σ level is $93 \mu\text{Jy beam}^{-1}$. The blue plus signs represent the positions of the two lensed images MACS0647-JD1 and MACS0647-JD2 as given in Tab. 2.

clumps of individual size $\leq 3 \text{ kpc}$. They present a spectrum for the simulated [CII] emission, where the FWHM of the main peak is $\sim 50 \text{ km s}^{-1}$, very similar to the 56 km s^{-1} of the LAE at $z=4.7$. This suggests that the width of the [CII] line is to first order determined by the gravitational potential of the clumps. The [CII] emission produced in the CNM follows the gravitational potential of the clumps, resulting in narrow emission lines associated with each clump. An ensemble of emitting clumps moving through the galaxy following the potential of the galaxy could combine and produce a broader line. Such behavior is not observed in the simulations, where just a small number of clumps dominate the [CII] emission.

We conclude that the adopted width of $\sim 50 \text{ km s}^{-1}$ for the [CII] line in LAEs agrees with recent observations and simulations. Nevertheless, we do not discard the possi-

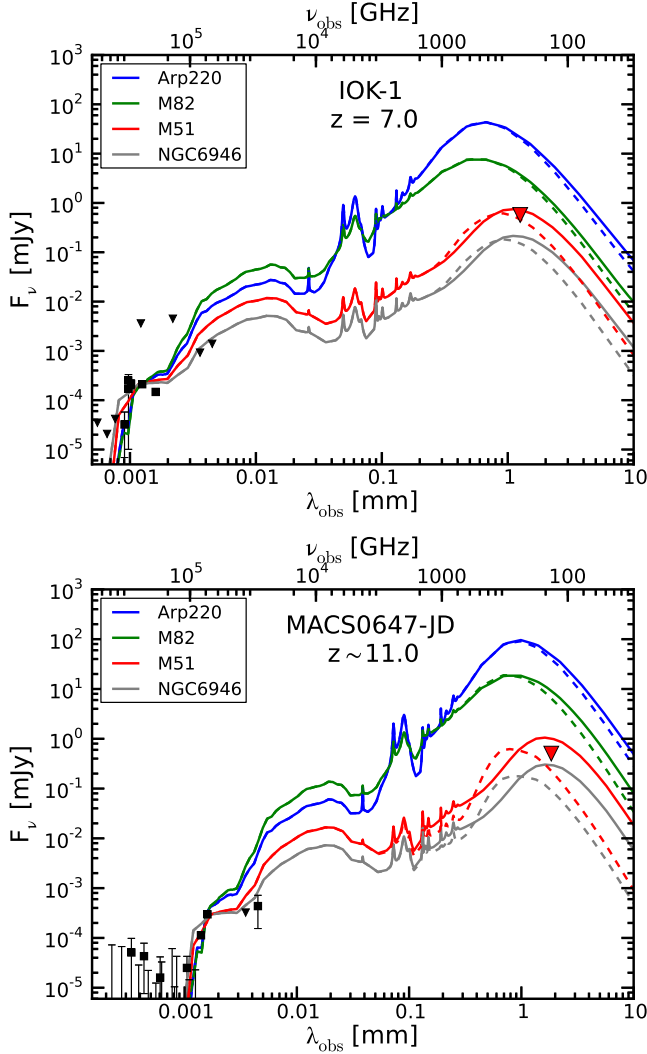


Figure 5. *Top:* Spectral energy distribution of IOK-1. The photometric points correspond to those measured by Iye et al. (2006); Ota et al. (2010); Cai et al. (2011); Ono et al. (2012). The red triangle corresponds to the 3σ upper limit given by the CARMA observations. The colored lines correspond to the SEDs of local galaxies shifted to the redshift of IOK-1 and scaled to the observations in the UV band. The dashed lines correspond to the observed SED of the local galaxies after the effects of the CMB on the observations are taken into account. *Bottom:* Spectral energy distribution of MACS0647-JD. The photometric points correspond to those presented by Coe et al. (2013). The SED of the galaxies follow the same prescription as in the upper panel. The red triangle corresponds to the 3σ upper limit calculated as the quadrature of the errors of the individual fluxes of JD1 and JD2, in the same way as the errors presented by Coe et al. (2013). The 1σ photometric uncertainty of the observations is 0.093 mJy, and the error of the added fluxes is 0.13 mJy.

bility of [C II] lines being broader than our assumption, but that the occurrence of unusually narrow lines in this population appears plausible.

4.2. CMB effects.

The Cosmic Microwave Background Radiation (CMB) emits as a black body with a temperature of $T_{\text{CMB}}^{z=0} = 2.7$ K. The temperature of the CMB increases linearly with $(1+z)$, becoming an important factor to take into account for observations of objects at high redshift. da Cunha et al. (2013) showed the effect of the CMB on

observations of high-redshift galaxies. Here we will follow the prescription formulated by da Cunha et al. (2013) to take into account the effects of the CMB in the continuum observations of galaxies at high redshift in the mm and sub-mm. We will apply this prescription to the SED of the local galaxies, as if they would be observed at a given redshift z .

The templates that we use are those presented by Silva et al. (1998) for the galaxies Arp 220, M82, M51 and NGC 6946. For the galaxies assume cold dust with temperature $T_{\text{dust}}^{z=0}$ and an emissivity index β . For Arp 220 we used $T_{\text{dust}}^{z=0} = 66.7$ K and $\beta = 1.86$ (Rangwala et al. 2011), for M82 $T_{\text{dust}}^{z=0} = 48$ K and $\beta = 1$ (Colbert et al. 1999), for M51 $T_{\text{dust}}^{z=0} = 24.9$ K and $\beta = 2$ (Mentuch Cooper et al. 2012) and for NGC 6946 we used $T_{\text{dust}}^{z=0} = 26$ K and $\beta = 1.5$ (Skibba et al. 2011). At a given redshift the CMB contributes to the dust heating such that the equilibrium temperature is:

$$T_{\text{dust}}(z) = \left((T_{\text{dust}}^{z=0})^{4+\beta} + (T_{\text{CMB}}^{z=0})^{4+\beta} [(1+z)^{4+\beta} - 1] \right)^{\frac{1}{4+\beta}}. \quad (1)$$

$T_{\text{dust}}^{z=0}$ is a measurement of the mean dust temperature as determined by a modified blackbody fit to an observed galaxy IR SED at $z = 0$, representing the total IR luminosity of the galaxy. As a representative fit, this is equally applicable to both optically thin galaxies and optically thick as in Arp 220. So long as the galaxy is transparent to the CMB radiation (true for even Arp 220), Eq. 1 holds. The additional heating by the CMB affects the SEDs such that the peak of the emission is shifted to a shorter wavelength and the total luminosity associated to the cold dust is higher by $[T_{\text{dust}}(z)/T_{\text{dust}}^{z=0}]^{(4+\beta)}$. We need to modify the intrinsic SED of the galaxies to include this new $T_{\text{dust}}(z)$. The flux density depends on the black body radiation for the given temperature,

$$F_{\nu/(1+z)} \propto B_{\nu}(T_{\text{dust}}(z)), \quad (2)$$

To include $T_{\text{dust}}(z)$ we have to apply the following factor to convert the intrinsic SED flux density to the emission associated with the new temperature $F_{\nu/(1+z)}^*$.

$$F_{\nu/(1+z)}^* = F_{\nu/(1+z)}^{\text{int}} \times \frac{B_{\nu}(T_{\text{dust}}(z))}{B_{\nu}(T_{\text{dust}}^{z=0})}. \quad (3)$$

This factor will only apply to the part of the SED that correspond to the emission of the cold dust. To accomplish this, we scale a modified black body (MBB) to the peak of the FIR emission of the SED at $T_{\text{dust}}^{z=0}$, and then use this MBB emission to estimate the ratio (R_{ν}) of emission associated with the cold dust at a given frequency,

$$R_{\nu} = \frac{K \nu^{\beta} B_{\nu}(T_{\text{dust}}^{z=0})}{F_{\nu}^{\text{int}}}, \quad (4)$$

where K is just the scaling factor. The flux density associated to the new temperature of the cold dust will be:

$$F_{\nu/(1+z)}^* = M_{\nu} \times F_{\nu/(1+z)}^{\text{int}} \quad (5)$$

with

$$M_\nu = \left[(1 - R_\nu) + R_\nu \times \frac{B_\nu(T_{\text{dust}}(z))}{B_\nu(T_{\text{dust}}^{z=0})} \right]. \quad (6)$$

Finally, following da Cunha et al. (2013), we have to take into account the effect of the CMB as an observing background. For this we have to multiply the flux associated with $T_{\text{dust}}(z)$ by C_ν ,

$$C_\nu = \left[1 - \frac{B_\nu(T_{\text{CMB}}(z))}{B_\nu(T_{\text{dust}}(z))} \right], \quad (7)$$

resulting in the flux observed of the galaxies as:

$$F_{\nu/(1+z)}^{\text{obs}} = C_\nu \times M_\nu \times F_{\nu/(1+z)}^{\text{int}}, \quad (8)$$

with $C_\nu \times M_\nu$ representing the effect of the CMB in the observations at a given frequency. The same corrections are derived when an optically thick emission is assumed, as in the case of Arp 220.

As we can see in Fig. 5, the effect of the CMB decreases the observable flux density at 2 mm by up to a factor of $5\times$ (in the case of M51) for the galaxy at $z \sim 11$, when the temperature of the CMB is higher, as expected. Also, the effect is higher for galaxies with a lower temperature of the cold dust. Galaxies with temperature of order of 25-30 K are more affected than those with temperature of 40-50 K. The CMB effects will be important for estimations of the flux densities of these type of galaxies in the continuum and for the correct interpretation of the observations.

The CMB effects on the [C II] line observations are similar to those on the continuum. The flux of an emission line observed against the CMB is:

$$\frac{S_{\nu/(1+z)}^{\text{obs}}}{S_{\nu/(1+z)}^{\text{int}}} = \left[1 - \frac{B_\nu(T_{\text{CMB}}(z))}{B_\nu(T_{\text{exc}})} \right], \quad (9)$$

with T_{exc} being the excitation temperature of the transition. For the case of local thermal equilibrium (LTE), when collisions dominate the excitation of the [C II] line, the excitation temperature of the transition is equal to the kinetic temperature of the gas (T_{kin}). The kinetic temperature varies for the different [C II] emission regions. Gas temperatures within PDRs are typically $T \sim 100 - 500$ K (Stacey et al. 2010), for the CNM $T \approx 250$ K, for the WNM $T \approx 5000$ K and for the ionized medium $T \approx 8000$ K (Vallini et al. 2013). Since the CMB temperature at $z = 6.5 - 11$ is much lower than the gas temperature of the [C II] emitting region, it will not contribute significantly to the [C II] excitation, but must be taken into account as the background against which the line flux is measured. In most of the [C II] emission regions, the temperatures are so high that the observed flux of the line against the CMB is similar to the intrinsic flux ($S_{\nu/(1+z)}^{\text{obs}}/S_{\nu/(1+z)}^{\text{int}} \approx 1$). For the extreme case where all the [C II] emission is being produced in PDRs with temperature of 100 K in a galaxy at $z = 11$, the observed flux (using Eq. 9) would be 90% of the intrinsic flux. We found this case very unlikely, since in low redshift galaxies the [C II] emission produced in PDRs is 50-70% of the total [C II] luminosity and the gas temperatures associated to the PDRs are higher (Crawford et al. 1985; Carral et al. 1994; Lord et al. 1996; Colbert et al.

1999). We conclude that the CMB effects on the [C II] line observations are negligible for our observations.

4.3. Spectral energy distribution of the galaxies.

Using the upper limits on the continuum, we compare the targets with the spectral energy distribution templates of local galaxies (SEDs). For the LAEs, the SEDs of the local galaxies are scaled to the flux of a near-IR filter that is not contaminated by the Ly α emission line. For MACS0647-JD, the filter used for the scaling is the one next to the Lyman Break. The photometry of IOK-1 and MACS0647-JD together with the SED of local galaxies are shown in Fig. 5. For SDF J132415.7+273058 and SDF J132408.3+271543 (not shown) the situation is very similar: the sources have a similar redshift, the continuum upper limits are comparable and the CMB effects are of the same order. Our upper limit for IOK-1 is comparable to the upper limit found by Walter et al. (2012b) using PdBI observations.

Using the SED of NGC 6946 as a template, we estimate the IR luminosity given the upper limit flux densities, similar to the approach shown by Walter et al. (2012b). We scale the SED of NGC 6946 to the 3 sigma upper limits of the mm observations and integrate from 8 μm to 1 mm (rest frame) to compute the IR luminosity.

The IR luminosity corresponding to this intrinsic SED and the SFR associated (Kennicutt 1998) are given in Tab. 1 for the LAEs and in Table 2 for MACS0647-JD. We note that estimating the IR luminosity using NGC 6946 without taking into account the CMB result in a significant underestimation of the luminosity upper limits. The IR luminosity limit corrected by the CMB of the LAEs at $z \sim 6.6$ is 35% higher than without correcting by the CMB. For IOK-1 at $z \sim 7$, the IR luminosity limit is a 50% higher than the estimation without correcting by the CMB. For MACS0647-JD at $z \sim 10.7$, the IR luminosity limit corrected for the CMB is ~ 3.5 times the IR luminosity limit not corrected by the CMB. For galaxies with cold dust temperature of ~ 25 K, the effect of the CMB on the observations is very important at high redshift, and it will significantly limit the feasibility of detecting not extremely starbursting galaxies in the IR continuum, it will not greatly affect the detectability of [C II] emission.

4.4. Ratio $L_{[\text{CII}]} / L_{\text{FIR}}$

Figure 6 presents our upper limits to $L_{[\text{CII}]} / L_{\text{FIR}}$ and L_{FIR} together with detections of [C II] in other galaxies. The arrows represent the region of possible values for $L_{[\text{CII}]} / L_{\text{FIR}}$ and L_{FIR} (integrated from 42.5 μm to 122.5 μm rest frame). If we used UV-based SFR estimates to infer L_{FIR} , our data points would move across the diagonal arrows towards the region where local galaxies are, putting our $L_{[\text{CII}]} / L_{\text{FIR}}$ upper limits close to the average value found for the local galaxies. The ratio $L_{[\text{CII}]} / L_{\text{FIR}}$ is a measure of how efficient the [C II] emission is in cooling the gas. The values presented for our targets, $\log(L_{[\text{CII}]} / L_{\text{FIR}}) \sim -2.9$, do not necessarily imply that [C II] is not efficient in cooling the gas in these galaxies, it is most likely a consequence of the galaxies having much lower FIR luminosities than our conservative upper limits. Different processes can affect the ratio $L_{[\text{CII}]} / L_{\text{FIR}}$. In galaxies with

low extinction and low metallicity, like in Haro 11, about 50% of the $[\text{C II}]$ emission arises from the diffuse ionized medium (Cormier et al. 2012). Variations on the fraction of $[\text{C II}]$ emission associated with the ionized medium will also affect the ratio $L_{[\text{C II}]} / L_{\text{FIR}}$. In some galaxies, the internal dust extinction can affect the ratio $L_{[\text{C II}]} / L_{\text{FIR}}$. In Arp 220, the dust is optically thick at $158 \mu\text{m}$ and can absorb part of the $[\text{C II}]$ emission, decreasing the ratio $L_{[\text{C II}]} / L_{\text{FIR}}$ (Rangwala et al. 2011).

Díaz-Santos et al. (2013) present the results of a survey of $[\text{C II}]$ in luminous infrared galaxies (LIRGs) observed with the PACS instrument on board the *Herschel Space Observatory*. They found a tight correlation between the ratio $L_{[\text{C II}]} / L_{\text{FIR}}$ and the far-IR $S_\nu(63 \mu\text{m}) / S_\nu(158 \mu\text{m})$ continuum color, independently of their L_{IR} . They found that the ratio decreases as the average temperature of dust increases, suggesting that the main observable linked to the variation of $L_{[\text{C II}]} / L_{\text{FIR}}$ is the average dust temperature. For the galaxies with dust temperatures $\sim 20\text{K}$ the average ratio is $\log(L_{[\text{C II}]} / L_{\text{FIR}}) \sim 10^{-2}$, suggesting that for galaxies like NGC 6946 with a dust temperature of $\approx 26\text{K}$, the ratio $L_{[\text{C II}]} / L_{\text{FIR}}$ should be on the same order of magnitude. Díaz-Santos et al. (2013) also found a correlation between $L_{[\text{C II}]} / L_{\text{FIR}}$ and luminosity surface density of the mid-IR emitting region ($\Sigma_{\text{IR}} = L_{\text{IR}} / \pi r_{\text{mid-IR}}^2$). LIRGs with lower $L_{[\text{C II}]} / L_{\text{FIR}}$ ratios are warmer and more compact. We can use this relation to find a rough estimation for $L_{[\text{C II}]} / L_{\text{FIR}}$ of our targets. As $r_{\text{mid-IR}}$ we use the size found in the UV observations of the targets. The half-light radius of IOK-1 is $\approx 0.62\text{ kpc}$ (Cai et al. 2011). The full width at half maximum size of SDF J132415.7+273058 and SDF J132408.3+271543 are ≈ 4.0 and 3.2 kpc respectively (Taniguchi et al. 2005). For MACS0647-JD the deconvolved half-light radius is $\lesssim 0.1\text{ kpc}$ (Coe et al. 2013). Using our L_{IR} upper limits as an approach to L_{IR} we can estimate Σ_{IR} . For IOK-1 the estimated ratio is $\log(L_{[\text{C II}]} / L_{\text{FIR}}) \sim -2.9$, for SDF J132415.7+273058 is $\log(L_{[\text{C II}]} / L_{\text{FIR}}) \sim -2.5$ and for SDF J132408.3+271543 is $\log(L_{[\text{C II}]} / L_{\text{FIR}}) \sim -2.6$. For the LAEs the average of $L_{[\text{C II}]} / L_{\text{FIR}}$ is similar to the average value for the local galaxies (Fig. 6). For MACS0647-JD the estimated ratio is $\log(L_{[\text{C II}]} / L_{\text{FIR}}) \sim -3.2$.

4.5. SFR- $L_{[\text{C II}]}$ Relation

In Fig. 7 we present our $L_{[\text{C II}]}$ upper limits with the UV-SFR estimated for the targets together with upper limits detections for published LAEs (Carilli et al. 2013; Kanekar et al. 2013; Ouchi et al. 2013). The black solid lines corresponds to the relation found by de Looze et al. (2011), with the gray area corresponding to 2σ scatter in the relation. Our upper limits for the $[\text{C II}]$ luminosity fall within the scatter of the SFR- $L_{[\text{C II}]}$, with the exception of SDF J132408.3+271543, where the upper limit falls above the relation due to the moderate depth of its observations. The detection of the LAE at $z=4.7$ ($\text{Ly}\alpha -1$) agree very well with the relation found by de Looze et al. (2011) using the UV-SFR estimated by Ohya et al. (2004). The upper limits for the lensed LAE at $z = 6.56$ HCM 6A and Himiko suggest that LAEs at $z > 6$ could fall below the relation found at low redshift. More observations are needed to clarify if there is an intrinsic differ-

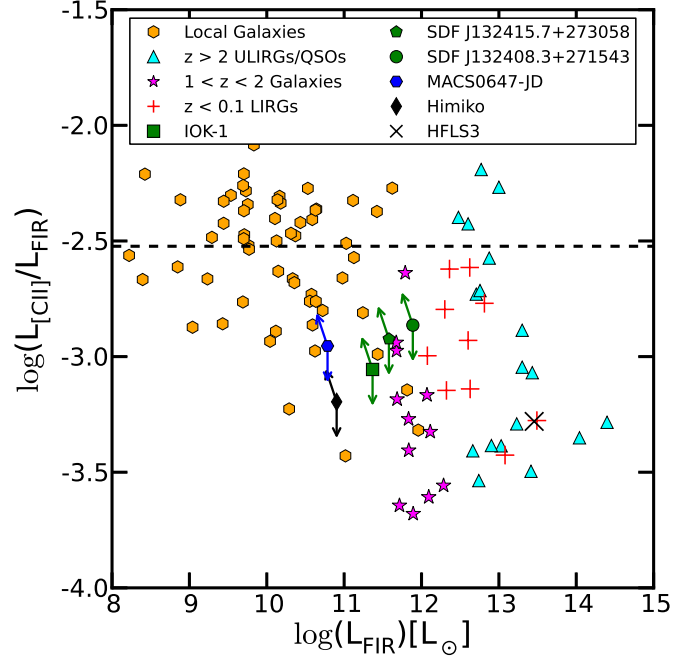


Figure 6. Ratio of the $[\text{C II}]$ luminosity to the FIR luminosity vs the FIR luminosity (integrated from $42.5 \mu\text{m}$ to $122.5 \mu\text{m}$ rest frame) for galaxies at different redshifts. The green symbols correspond to the upper limits of the LAEs presented here. The blue hexagon corresponds to the upper limit of MACS0647-JD using the most sensitive setup. The FIR luminosities for the galaxies are upper limits estimated from the observations including the CMB effects. The black diamond corresponds to the upper limit for Himiko with ALMA observations (Ouchi et al. 2013). The horizontal dashed line is the average value for $L_{[\text{C II}]} / L_{\text{FIR}}$ on the local galaxies. (Malhotra et al. 2001; Negishi et al. 2001; Luhman et al. 2003; Iono et al. 2006; Maiolino et al. 2009; Walter et al. 2009; Stacey et al. 2010; Ivison et al. 2010; Wagg et al. 2010; Cox et al. 2011; De Breuck et al. 2011; Swinbank et al. 2012; Venemans et al. 2012; Walter et al. 2012a; Wang et al. 2013; Riechers et al. 2013; Ouchi et al. 2013)

ence between the LAEs at $z \sim 4.5$ with the higher redshift population. The high magnification of MACS0647-JD allows us to explore an UV-SFR one order of magnitude lower than the ones of the LAEs, showing the advantage of observing lensed galaxies to cover the intrinsically faint population at high redshift.

4.6. IOK-1 Models

Using the same procedure presented in Vallini et al. (2013) for the $[\text{C II}]$ emission of Himiko, we estimate the emission of $[\text{C II}]$ for IOK-1 at $z \sim 7$. For this simulation, the star formation rate was set to $20\text{ M}_\odot\text{yr}^{-1}$ and a stellar population age of 10 Myr . The metallicity was set to solar to have a conservative estimation of the $[\text{C II}]$ emission. The simulation does not include the emission from PDRs and should be seen as a lower limit. In Fig. 8, we show the $[\text{C II}]$ emission produced by the three modeled phases, cold neutral medium (CNM), warm neutral medium (WNM) and the ionized medium. Most of the $[\text{C II}]$ emission comes from the CNM ($\sim 50\%$), the rest is coming from the WNM ($\sim 20\%$) and from the ionized medium ($\sim 30\%$). For comparison, in Himiko, 95% of the emission is produced in the CNM and the rest in the WNM. No emission from the ionized medium was modeled in the simulation of Himiko (Vallini et al. 2013). We can also see in the emission that the FWHM

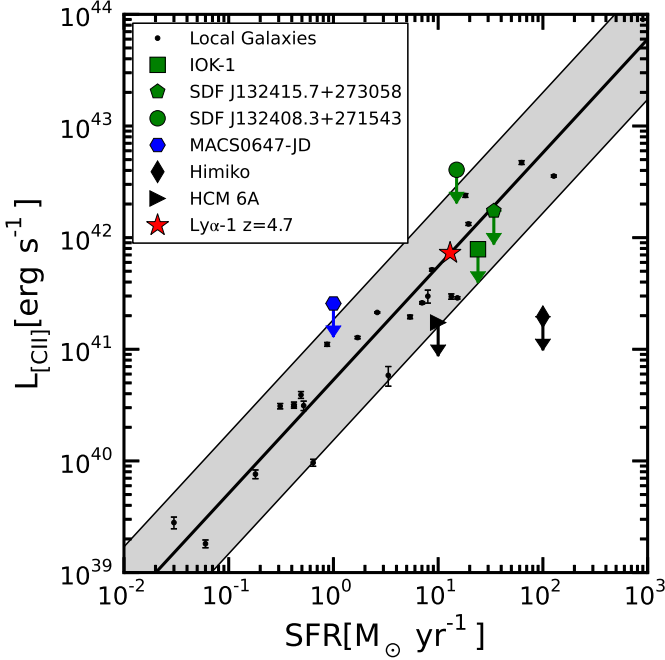


Figure 7. Relation of the [CII] luminosity with the UV-derived star formation rate of galaxies. The black solid lines correspond to the relation found by de Looze et al. (2011), with the gray area corresponding to 2σ of the scatter in the relation. The black dots with error bars correspond to the data used to find the relation of [CII] - SFR. The green circle, square and pentagon correspond to the LAEs with the [CII] upper limits presented in this paper assuming the star formation rate estimated from the UV fluxes. The blue hexagon corresponds to the [CII] upper limit of MACS0647-JD with based in the most sensitive setup and the star formation rate estimated from the UV fluxes. The red star corresponds to the LAE detected with ALMA at $z \sim 4.7$ (Carilli et al. 2013). The black triangle corresponds to the upper limit of the [CII] emission found for HCM-6A by Kanekar et al. (2013). The black diamond corresponds to the upper limit of the [CII] emission found for Himiko by Ouchi et al. (2013).

of the main peak is $\sim 50 \text{ km s}^{-1}$, just as expected.

In Fig. 9, we present the integrated flux of [CII] for a different combination of metallicities and stellar population ages. This shows a strong dependency on the metallicity, which is expected, since it is treated linearly with the abundance of [CII] in the gas. The second main feature of this results is the dependency with the stellar population age. Here we assumed a continuum star formation rate of $20 \text{ M}_{\odot} \text{ yr}^{-1}$, for the older stellar populations there is a higher amount of heating photons coming from the UV part of the spectrum. This is a result of using a continuum star formation mode, for a given SFR, older populations have more time generating young UV emitting stars. These extra heating photons avoid the cooling of the gas, which decrease the amount of gas in the cold neutral medium, where most of the [CII] emission is produced.

4.7. Spectral Resolution

For a Gaussian emission line, with a FWHM of 50 km s^{-1} observed at a channel resolution of 200 km s^{-1} , emission lines will be significantly diluted. In the best case scenario of the line falling completely in one channel, we will recover 38% of the peak flux density of the line. This suggests to carry out observations a sufficiently high spectral resolution. E.g. with a line of FWHM of 50

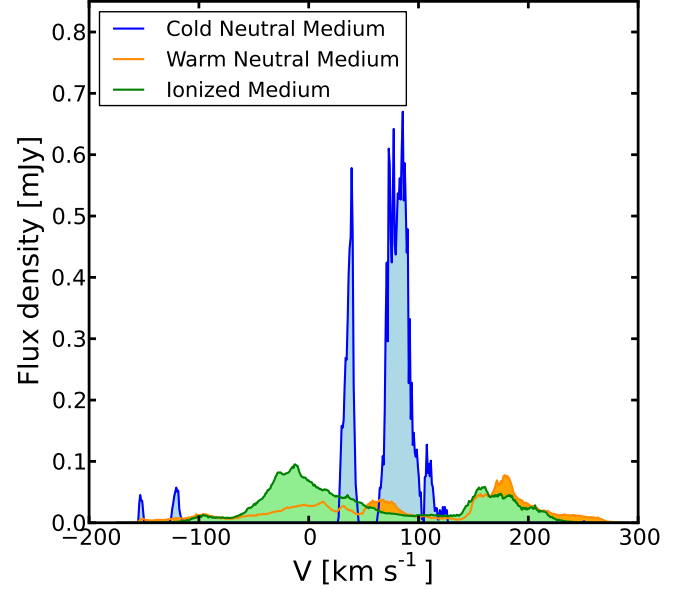


Figure 8. Simulated [CII] spectrum of a galaxy similar to IOK-1 at $z \sim 7$. The parameters set for this simulation were a SFR of $20 \text{ M}_{\odot} \text{ yr}^{-1}$, and stellar population age of 10 Myr and a solar metallicity. The blue spectrum corresponds to the emission produced in the cold neutral medium, the orange spectrum corresponds to the emission produced in the warm neutral medium and the green spectrum corresponds to the emission produced in the ionized medium. The main peak (at $\sim 80 \text{ km s}^{-1}$) of the cold neutral medium has a FWHM of $\sim 50 \text{ km s}^{-1}$. For more details on the simulations of [CII] emission in high redshift galaxies see Vallini et al. (2013).

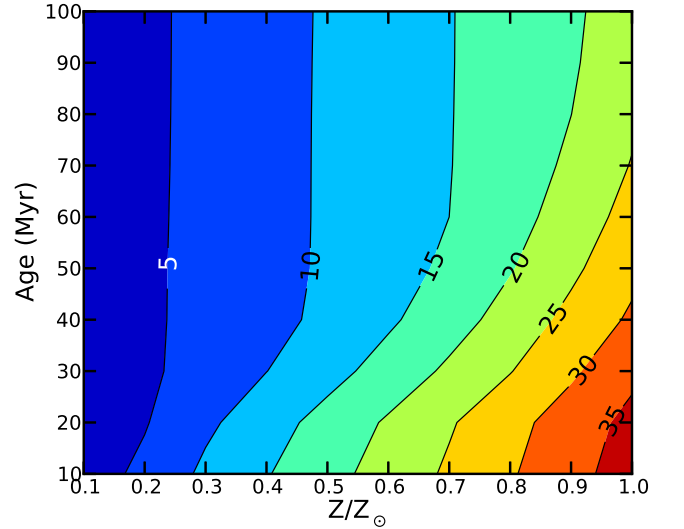


Figure 9. Contour plot of the integrated [CII] flux of IOK-1 in mJy km s^{-1} for different simulation conditions. As comparison, our upper limit for integrated flux of IOK-1 is $175 \text{ mJy km s}^{-1}$. The two independent parameters are the stellar population age and the metallicity of the gas. The flux is integrated over the whole area of the cube and in a channel resolution of 500 km s^{-1} around the peak of the emission. The integrated flux is a conservative upper limit for the different parameters. We can see from the contour plot that the [CII] emission is very sensitive to the metallicity of the galaxy, and in a less significant way to the age of the stellar population. The different ages correspond to a different amount of heating photons coming from the young stars, which is critical for the cooling of the gas.

kms^{-1} and a channel resolution of 10 km s^{-1} , we expect to recover 97% of the peak flux density of the line.

4.8. Atomic Mass Estimation

We use Equation 1 from (Hailey-Dunsheath et al. 2010) to give rough upper limits to the atomic mass associated with PDRs in our targets (Assuming all $[\text{C II}]$ would arise from PDRs). As approach to the PDRs conditions we use the result of Vallini et al. (2013) for the temperature and density in the CNM of Himiko, $n = 5 \times 10^4 \text{ cm}^{-3}$ and $T=250 \text{ K}$. Using our upper limits for $[\text{C II}]$ we obtain the following upper limits to the atomic mass: For IOK-1 $M_{\text{HI}} \lesssim 2 \times 10^8 M_{\odot}$, for SDF J132415.7+273058 $M_{\text{HI}} \lesssim 4 \times 10^8 M_{\odot}$, for SDF J132408.3+271543 $M_{\text{HI}} \lesssim 1 \times 10^9 M_{\odot}$ and for MACS0647-JD $M_{\text{HI}} \lesssim 6 \times 10^7 M_{\odot}$. Assuming that the mass of atomic gas is similar to the mass of molecular gas, we can compare our upper limits with the measurements of similar galaxies at lower redshift.

The only molecular gas masses measured in high redshift UV-selected star-forming galaxies come from the detection of CO transition lines in lensed LBGs. The measured values are, $\sim 4 \times 10^8 M_{\odot}$, $\sim 9 \times 10^8 M_{\odot}$ and $\sim 1 \times 10^9 M_{\odot}$ for MS 1512-cB58 ($z = 2.73$), the cosmic eye ($z = 3.07$) and MS1358-arc ($z = 4.9$) respectively (Coppin et al. 2007; Riechers et al. 2010; Livermore et al. 2012). Our upper limits for the LAEs are similar to the values estimated for the observed LBGs. For MACS0647-JD our upper limit for the molecular mass is at least $8 \times$ lower than in the observed LBGs.

Using the UV-SFR relation we can estimate the gas depletion timescales for our targets, assuming $\tau_{\text{dep}} = M_{\text{gas}}/\text{SFR}_{\text{UV}}$. We estimate upper limits for the depletion time of $\lesssim 8 \text{ Myr}$, $\lesssim 11 \text{ Myr}$ and $\lesssim 66 \text{ Myr}$ for IOK-1, SDF J132415.7+273058 and SDF J132408.3+271543 respectively. For MACS0647-JD the depletion time is $\lesssim 60 \text{ Myr}$. The estimated depletion times for the observed lower redshift lensed LBGs are within the range of $\sim 7 - 24 \text{ Myr}$, similar to our upper limits. The depletion times for the LAEs are consistent with the ages estimated for the young population of LAEs at $z \sim 4.5$ of $< 15 \text{ Myr}$ found by Finkelstein et al. (2009) and to the simulated LAEs at ~ 3.1 with ages $< 100 \text{ Myr}$ (Shimizu et al. 2011). The depletion times of the LBGs are consistent with the LBG-phase predicted duration of $20 - 60 \text{ Myr}$ (González et al. 2012).

Saintonge et al. (2013) presented molecular gas masses and depletion timescales for a sample of lensed star forming galaxies at $z = 1.4 - 3.1$. The range of measured molecular gas masses is $5.6 \times 10^9 - 4 \times 10^{11} M_{\odot}$ and of depletion timescales is $127 - 1089 \text{ Myr}$. The longer depletion timescales measured for the lower- z sources could indicate that they experience less ‘extreme’ bursts of star formation in comparison to our $z > 6.5$ sample. Although, assuming a higher molecular-to-atomic gas ratio (of at least 5) would put our upper limits within the values measured by Saintonge et al. (2013).

5. SUMMARY AND OUTLOOK.

We have presented a search for $[\text{C II}]$ emission in three LAEs at $z \sim 7$ and in a LBG at $z \sim 11$ using CARMA and the PdBI. We summarize our results and conclusions as follows:

1. We have not detected $[\text{C II}]$ emission line any of our targets. Given the recent observational results and simulations of the $[\text{C II}]$ emission in high redshift LAE, we adopt a line width of 50 km s^{-1} for the $[\text{C II}]$ emission. We put constraints on the luminosity of the line for the targets. For the LAEs the 3σ $L_{[\text{C II}]}$ upper limit are < 2.05 , < 4.52 and $< 10.56 \times 10^8 L_{\odot}$ for IOK-1, SDF J132415.7+273058 and SDF J132408.3+271543 respectively. Our $[\text{C II}]$ upper limits are consistent with the relation of $\text{SFR}-L_{[\text{C II}]}$ found by de Looze et al. (2011). The 3σ upper limit in the $[\text{C II}]$ luminosity of MACS0647-JD is $< 5.27 \times 10^7 \times (\mu/15)^{-1} L_{\odot}$ (Assuming that the redshift of the galaxy is within the most sensitive setup).
2. No detection of the FIR continuum is found at a wavelength of $158 \mu\text{m}$ rest frame for any of the 4 targets. Assuming a spectral energy distribution template for the local galaxy NGC 6946 as a template for the high redshift galaxies observed here, we present conservative upper limits for the FIR luminosity. We find < 2.33 , 3.79 and $7.72 \times 10^{11} L_{\odot}$ as upper limits for IOK-1, SDF J132415.7+273058 and SDF J132408.3+271543 respectively, these values account for the effect of the CMB on the observations. For MACS0647-JD, the upper limit in the FIR luminosity is $< 6.1 \times 10^{10} \times (\mu/15)^{-1} L_{\odot}$, after correcting for the CMB and the lensing magnification.
3. We present the results of simulations supporting the brightest component of the $[\text{C II}]$ line having a width of the order of 50 km s^{-1} . Here we want to emphasize the necessity of resolving such emission lines in future ALMA observations, to not loose signal-to-noise ratio, by selecting a channel resolution that is too low.
4. The effect of the CMB must to be taken into account in attempts to detect the FIR continuum in galaxies at high redshift. The heating of cold dust by CMB photons can shift the peak of the FIR continuum to values up to a ~ 400 microns for galaxies with temperature of $\sim 25 \text{ K}$ and redshift of $z \sim 11$. We emphasize that not including the effects of the CMB on the observations results in an underestimation of the FIR luminosities for the targets. The CMB corrected FIR luminosity limits are 35% higher than those without CMB correction at $z \sim 6.6$, 50% higher at $z \sim 7$, and 350% higher at $z \sim 11$ for a $T = 26 \text{ K}$.
5. Simulations are already showing us that the task of detecting $[\text{C II}]$ in high redshift galaxies is going to be difficult even with ALMA, as confirmed by the recent sensitive non-detection of Himiko by Ouchi et al. (2013). Accordingly to our IOK-1 simulations, a key parameter for the $[\text{C II}]$ emission in LAEs is the metallicity, as we discussed in Sect. 4.6. If these simulations were applicable to all high redshift LAEs, we should first try to detect

[C II] in the LAEs with the highest metallicity. Estimating the metallicity of LAEs at high redshift is not an easy task, however, Cowie et al. (2011) found that for the sample of LAEs discovered by the Galaxy Evolution Explorer (GALEX) grism in the redshift range of $z = 0.195 - 0.44$, there is an anti-correlation of the equivalent width of the H α emission line with metallicity. Higher EW(H α) sources all have lower metallicities, bluer colors, smaller sizes, and less extinction. Cowie et al. (2011) also found a broad general trend that for higher EW(H α), the EW(1y α) is also higher. If we assume that these relations are valid for the LAEs at high redshift, and that the goal is to observe the LAE with the highest metallicity possible, it may be best to target the brightest LAE in the UV but with the lowest Ly α equivalent width. Lyman-break galaxies with Ly α detection may thus be ideal targets for [C II] searches at high redshift.

We thank the referee for his/her useful comments and suggestions which significantly improved the quality of this paper. We thank Brent Groves for the discussion on the effects of the CMB. Support for CARMA construction was derived from the states of California, Illinois, and Maryland, the James S. McDonnell Foundation, the Gordon and Betty Moore Foundation, the Kenneth T. and Eileen L. Norris Foundation, the University of Chicago, the Associates of the California Institute of Technology, and the National Science Foundation. Ongoing CARMA development and operations are supported by the National Science Foundation under a cooperative agreement, and by the CARMA partner universities. Based on observations with the IRAM Plateau de Bure Interferometer. IRAM is supported by INSU/CNRS (France), MPG (Germany) and IGN (Spain). LI and JG obtained partial support from CATA, Conicyt Basal program. LI and JG acknowledge support from FON-DAP “Centro de Astrofísica” 15010003. LI thanks the collaboration of the CLASH team.

REFERENCES

- Brammer, G. B., van Dokkum, P. G., Illingworth, G. D., et al. 2013, *ApJ*, 765, L2
- Bouwens, R. J., Illingworth, G. D., Labbe, I., et al. 2011, *Nature*, 469, 504
- Cai, Z., Fan, X., Jiang, L., et al. 2011, *ApJ*, 736, L28
- Capak, P. L., Faisst, A., Vieira, J. D., et al. 2013, arXiv:1307.4089
- Carilli, C. L., Riechers, D., Walter, F., et al. 2013, *ApJ*, 763, 120
- Carilli, C. L., & Walter, F. 2013, *ARA&A*, 51, 105
- Carral, P., Hollenbach, D. J., Lord, S. D., et al. 1994, *ApJ*, 423, 223
- Coe, D., Zitrin, A., Carrasco, M., et al. 2013, *ApJ*, 762, 32
- Colbert, J. W., Malkan, M. A., Clegg, P. E., et al. 1999, *ApJ*, 511, 721
- Coppin, K. E. K., Swinbank, A. M., Neri, R., et al. 2007, *ApJ*, 665, 936
- Cormier, D., Leboutteiller, V., Madden, S. C., et al. 2012, *A&A*, 548, A20
- Cowie, L. L., Barger, A. J., & Hu, E. M. 2011, *ApJ*, 738, 136
- Cox, P., Krips, M., Neri, R., et al. 2011, *ApJ*, 740, 63
- Crawford, M. K., Genzel, R., Townes, C. H., & Watson, D. M. 1985, *ApJ*, 291, 755
- da Cunha, E., Groves, B., Walter, F., et al. 2013, *ApJ*, 766, 13
- Dayal, P., & Ferrara, A. 2012, *MNRAS*, 421, 2568
- De Breuck, C., Maiolino, R., Caselli, P., et al. 2011, *A&A*, 530, L8
- de Looze, I., Baes, M., Bendo, G. J., Cortese, L., & Fritz, J. 2011, *MNRAS*, 416, 2712
- Diaz-Santos, T., Armus, L., Charmandaris, V., et al. 2013, arXiv:1307.2635
- Ellis, R. S., McLure, R. J., Dunlop, J. S., et al. 2013, *ApJ*, 763, L7
- Finkelstein, S. L., Rhoads, J. E., Malhotra, S., Pirzkal, N., & Wang, J. 2007, *ApJ*, 660, 1023
- Finkelstein, S. L., Rhoads, J. E., Malhotra, S., & Grogan, N. 2009, *ApJ*, 691, 465
- Fontana, A., Vanzella, E., Pentericci, L., et al. 2010, *ApJ*, 725, L205
- Gallerani, S., Neri, R., Maiolino, R., et al. 2012, *A&A*, 543, A114
- Gawiser, E., van Dokkum, P. G., Gronwall, C., et al. 2006, *ApJ*, 642, L13
- González, J. E., Lacey, C. G., Baugh, C. M., Frenk, C. S., & Benson, A. J. 2012, *MNRAS*, 423, 3709
- Hailey-Dunsheath, S., Nikola, T., Stacey, G. J., et al. 2010, *ApJ*, 714, L162
- Hashimoto, T., Ouchi, M., Shimasaku, K., et al. 2013, *ApJ*, 765, 70
- Iono, D., Yun, M. S., Elvis, M., et al. 2006, *ApJ*, 645, L97
- Israel, F. P., Maloney, P. R., Geis, N., et al. 1996, *ApJ*, 465, 738
- Ivison, R. J., Swinbank, A. M., Swinyard, B., et al. 2010, *A&A*, 518, L35
- Iye, M., Ota, K., Kashikawa, N., et al. 2006, *Nature*, 443, 186
- Jiang, L., Egami, E., Mechtley, M., et al. 2013a, arXiv:1303.0024
- Jensen, H., Laursen, P., Mellema, G., et al. 2013, *MNRAS*, 428, 1366
- Kanekar, N., Wagg, J., Ram Chary, R., & Carilli, C. L. 2013, *ApJ*, 771, L20
- Kennicutt, R. C., Jr. 1998, *ARA&A*, 36, 189
- Lai, K., Huang, J.-S., Fazio, G., et al. 2008, *ApJ*, 674, 70
- Livermore, R. C., Swinbank, A. M., Smail, I., et al. 2012, *ApJ*, 758, L35
- Lord, S. D., Hollenbach, D. J., Haas, M. R., et al. 1996, *ApJ*, 465, 703
- Luhman, M. L., Satyapal, S., Fischer, J., et al. 2003, *ApJ*, 594, 758
- Madden, S. C., Poglitsch, A., Geis, N., Stacey, G. J., & Townes, C. H. 1997, *ApJ*, 483, 200
- Maiolino, R., Cox, P., Caselli, P., et al. 2005, *A&A*, 440, L51
- Maiolino, R., Caselli, P., Nagao, T., et al. 2009, *A&A*, 500, L1
- Malhotra, S., Kaufman, M. J., Hollenbach, D., et al. 2001, *ApJ*, 561, 766
- Mentuch Cooper, E., Wilson, C. D., Foyle, K., et al. 2012, *ApJ*, 755, 165
- Negishi, T., Onaka, T., Chan, K.-W., & Roellig, T. L. 2001, *A&A*, 375, 566
- Ohya, Y., Taniguchi, Y., & Shioya, Y. 2004, *AJ*, 128, 2704
- Ono, Y., Ouchi, M., Mobasher, B., et al. 2012, *ApJ*, 744, 83
- Ota, K., Iye, M., Kashikawa, N., et al. 2008, *ApJ*, 677, 12
- Ota, K., Ly, C., Malkan, M. A., et al. 2010, *PASJ*, 62, 1167
- Oteo, I., Bongiovanni, A., Pérez García, A. M., et al. 2012a, *A&A*, 541, A65
- Oteo, I., Bongiovanni, A., Pérez García, A. M., et al. 2012b, *ApJ*, 751, 139
- Ouchi, M., Ellis, R., Ono, Y., et al. 2013, arXiv:1306.3572
- Pentericci, L., Fontana, A., Vanzella, E., et al. 2011, *ApJ*, 743, 132
- Petitjean, P., Pécontal, E., Valls-Gabaud, D., & Chariot, S. 1996, *Nature*, 380, 411
- Postman, M., Coe, D., Benítez, N., et al. 2012, *ApJS*, 199, 25
- Rangwala, N., Maloney, P. R., Glenn, J., et al. 2011, *ApJ*, 743, 94
- Rhoads, J. E., Hibon, P., Malhotra, S., Cooper, M., & Weiner, B. 2012, *ApJ*, 752, L28
- Riechers, D. A., Carilli, C. L., Walter, F., & Momjian, E. 2010, *ApJ*, 724, L153
- Riechers, D. A., Bradford, C. M., Clements, D. L., et al. 2013, *Nature*, 496, 329
- Saintonge, A., Lutz, D., Genzel, R., et al. 2013, *ApJ*, 778, 2
- Sault, R. J., Teuben, P. J., & Wright, M. C. H. 1995, *Astronomical Data Analysis Software and Systems IV*, 77, 433
- Schenker, M. A., Stark, D. P., Ellis, R. S., et al. 2012, *ApJ*, 744, 179
- Shibuya, T., Kashikawa, N., Ota, K., et al. 2012, *ApJ*, 752, 114
- Shimizu, I., Yoshida, N., & Okamoto, T. 2011, *MNRAS*, 418, 2273
- Silva, L., Granato, G. L., Bressan, A., & Danese, L. 1998, *ApJ*, 509, 103
- Skibba, R. A., Engelbracht, C. W., Dale, D., et al. 2011, *ApJ*, 738, 89

- Solomon, P. M., Downes, D., & Radford, S. J. E. 1992, *ApJ*, 387, L55
- Stacey, G. J., Geis, N., Genzel, R., et al. 1991, *ApJ*, 373, 423
- Stacey, G. J., Hailey-Dunsheath, S., Ferkinhoff, C., et al. 2010, *ApJ*, 724, 957
- Stark, D. P., Ellis, R. S., Chiu, K., Ouchi, M., & Bunker, A. 2010, *MNRAS*, 408, 1628
- Swinbank, A. M., Karim, A., Smail, I., et al. 2012, *MNRAS*, 427, 1066
- Taniguchi, Y., Ajiki, M., Nagao, T., et al. 2005, *PASJ*, 57, 165
- Vallini, L., Gallerani, S., Ferrara, A., & Baek, S. 2013, *MNRAS*, 433, 1567
- Valtchanov, I., Virdee, J., Ivison, R. J., et al. 2011, *MNRAS*, 415, 3473
- Vanzella, E., Pentericci, L., Fontana, A., et al. 2011, *ApJ*, 730, L35
- Venemans, B. P., McMahon, R. G., Walter, F., et al. 2012, *ApJ*, 751, L25
- Wagg, J., Carilli, C. L., Wilner, D. J., et al. 2010, *A&A*, 519, L1
- Wagg, J., Wiklind, T., Carilli, C. L., et al. 2012, *ApJ*, 752, L30
- Walter, F., Riechers, D., Cox, P., et al. 2009, *Nature*, 457, 699
- Walter, F., Decarli, R., Carilli, C., et al. 2012a, *Nature*, 486, 233
- Walter, F., Decarli, R., Carilli, C., et al. 2012b, *ApJ*, 752, 93
- Wang, R., Wagg, J., Carilli, C. L., et al. 2013, *arXiv:1302.4154*
- Willott, C. J., Omont, A., & Bergeron, J. 2013, *ApJ*, 770, 13
- Zheng, W., Postman, M., Zitrin, A., et al. 2012, *Nature*, 489, 406